Supplemental Document

Optics EXPRESS

Structuring of perovskite-silicon tandem solar cells for reduced reflectance and thermalization losses: supplement

ADRIAN CALLIES,[1,*] MARIO HANSER,[1] JAN CHRISTOPH GOLDSCHMIDT,[2] BENEDIKT BLÄSI,[1] AND OLIVER HÖHN[1]

[1] *Fraunhofer Institute for Solar Energy Systems ISE, Heidenhofstraße 2, 79110 Freiburg, Germany*
[2] *Philipps-University Marburg, Renthof 7, 35032 Marburg, Germany*
[*] *adrian.callies@ise.fraunhofer.de*

Supplement DOI: https://doi.org/10.6084/m9.figshare.22829114

Parent Article DOI: https://doi.org/10.1364/OE.491371

Supplementary Document for

Structuring of Perovskite-Silicon Tandem Solar Cells for Reduced Reflectance and Thermalization Losses

ADRIAN CALLIES[1,*], MARIO HANSER[1], JAN CHRISTOPH GOLDSCHMIDT[2], BENEDIKT BLÄSI[1] AND OLIVER HÖHN[1]

[1]Fraunhofer Institute for Solar Energy Systems ISE, Heidenhofstraße 2, 79110 Freiburg, Germany
[2]Philipps-University Marburg, Renthof 7, 35032 Marburg, Germany
**adrian.callies@ise.fraunhofer.de*

S1. Feature Geometries in Use

Within this study, three different unit cell geometries have been used and their height H and unit cell period P have been varied. They are illustrated in Fig. 1 and **Error! Reference source not found.** shows the equation giving the z-coordinate at each point of the unit cell. Also, the fill factor is given, which states the volume occupied by this geometry relative to a bulk material with the same height. Note that when using RCWA, these structures are approximated using a step approximation.

Table S1. Mathematical description and fill factor for the unit cell geometries used within this study.

Geometry	Equation	Fill Factor
Sinusoidal	$z = H \cdot \cos\left(\frac{2\pi \cdot \max(\lvert x\rvert, \lvert y\rvert)}{P}\right)$	0.30
Quadratic	$z = H - \max(\lvert x\rvert, \lvert y\rvert)^2 \cdot \frac{4S}{P^2}$	0.50
Pyramidal	$z = H \cdot \left(1 - \frac{\lvert x+y\rvert + \lvert x-y\rvert}{P}\right)$	0.33

S2. Convergence Analysis

For the two simulation parameters of considered evanescent orders and layer height in z-direction, a convergence analysis has been conducted. For this, at wavelengths 400 nm, 600 nm, 800 nm, 1000 nm and 1200 nm, both reflection and transmission have been calculated for a system similar to Figure1b with a period of 500 nm and structure heights of 250 nm and 500 nm. Layer height was varied between 5 nm and 60 nm (finally used: 10 nm), number of evanescent orders between 0 and 10 (finally used: 3). The results are shown in Fig. S1.

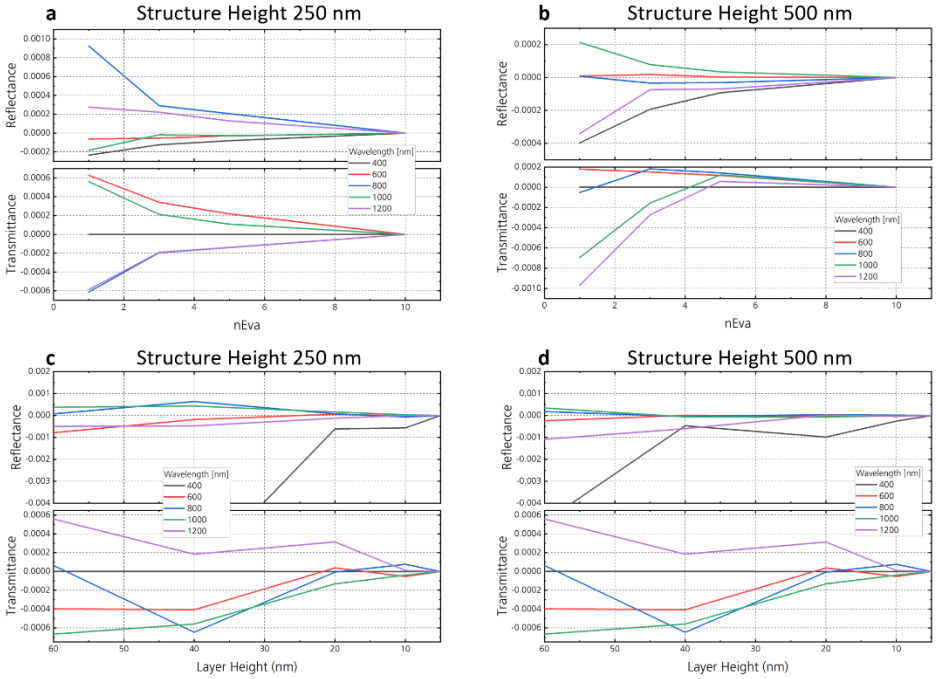

Fig. S1. Convergence Analysis for a the RCWA calculation. A representative system with a structure at the air-perovskite interface has been chosen, with a structure period of 500 nm and structure heights of 250 nm (a, c)/500 nm (b, d). Both the number of considered evanescent orders (a, b) and the layer height (c, d) has been varied.

S3. Perovskite Bandgap Determination

The bandgap of the used perovskite dataset [1,2] has been determined using two methods: From the Tauc plot according to [3] and from the derivative of the absorptance according to [4]. Both methods result in a bandgap of 1.72 eV, as visible in Fig. S2. The bandgap given in [5] is 1.67 eV.

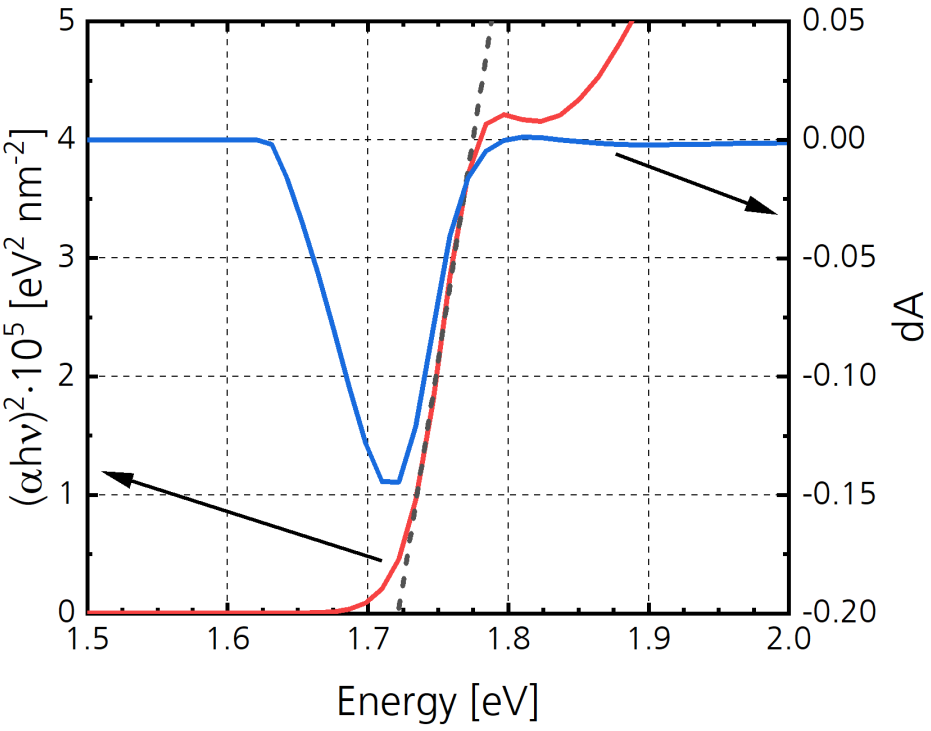

Figure S2. Tauc plot and derivative of the absorptance of the used perovskite dataset. Used to determine the bandgap at 1.72 eV with both methods.

S4. Spatial Distribution of Absorbed Intensity for the Same Geometry at Both Interfaces with a Larger Structure Height and Period of 650 nm

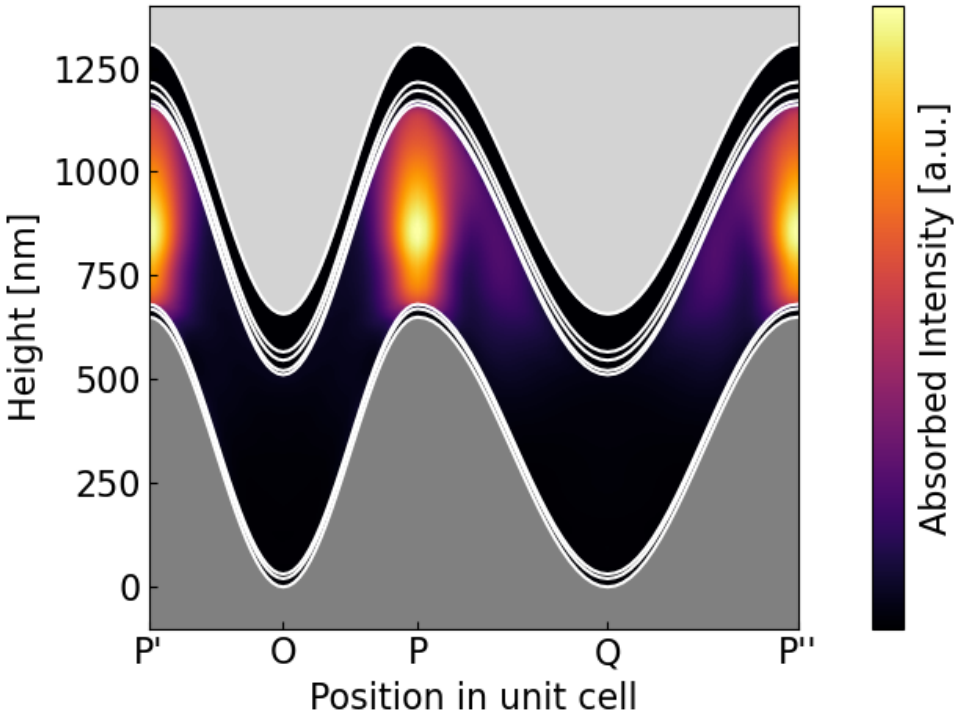

Figure S3. Spatial distribution of the absorbed intensity for a configuration with the same geometry at both interfaces, with both period and structure height set at 650 nm.

S5. Literature Comparison and Perspective of the Simulation Model in Use

Throughout this work, established simulation methods have been applied. The RCWA method and implementation [6] used has been successfully applied to describe experimental data of nanostructured interfaces in multiple publications [7–9]. The applicability to the perovskite top solar cell was verified by comparing simulation and experimental results from [10] in Fig. S4. There, a good agreement is observed for the top cell, while less reflection is observed for the wavelength region of the silicon bottom cell. This is due to the simplified, but well established [8,11], model in use, which includes less interfaces with refractive index changes within the silicon bottom cell. This is equivalent to using a different bottom cell concept in experiment. While there is an offset, the shape of the curve is similar except for a wavelength shift of the maxima by around 35 nm.

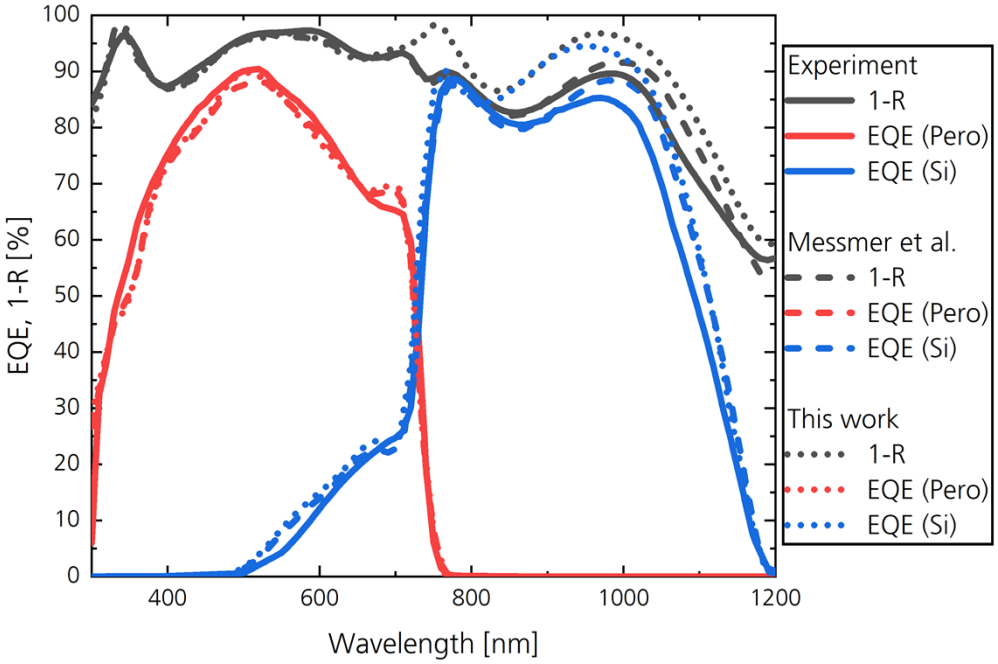

Figure S4. Comparison of reflection and absorption results achieved in experiment, with the simulation method of [10] and the simulation method used within this work for the stack described in [10].

S6. Material Volume Necessary to Achieve Same Reduction in Thermalization Losses as with Optimized Structure.

Across this paper, an estimation of the thermalization losses is done by comparing the value of absorptance by the perovskite at a wavelength of 700 nm. This reference value is chosen because all systems considered exhibit almost no reflection at this wavelength and it is close to the bandgap of the used perovskite, where transmission losses occur most prominently. The absorptance enhancement achieved by the use of optimized structuring can equivalently be achieved by increasing the material thickness of the perovskite absorber. For both the flat and random pyramid case, the increase in material thickness to achieve the same value of absorptance in the top cell at 700 nm as in the case of optimized nanostructures has been calculated in Figure S. In the figure, the material thickness normal to the macroscopic sample surface is varied, to provide a measure for the material volume in use consistent with the rest of the paper. For the random pyramids case, this means that the thickness normal to the pyramid surface is by a factor of 1.73 smaller than the thickness given on the axis.
To achieve a similar reduction in transmission/thermalization losses as with the optimized nanostructure, on a planar substrate a perovskite an increase in thickness from 480 to 700 nm is necessary, while for pyramids a thickness of 1150 nm normal to the macroscopic surface or 665 nm normal to the pyramid surface is necessary.

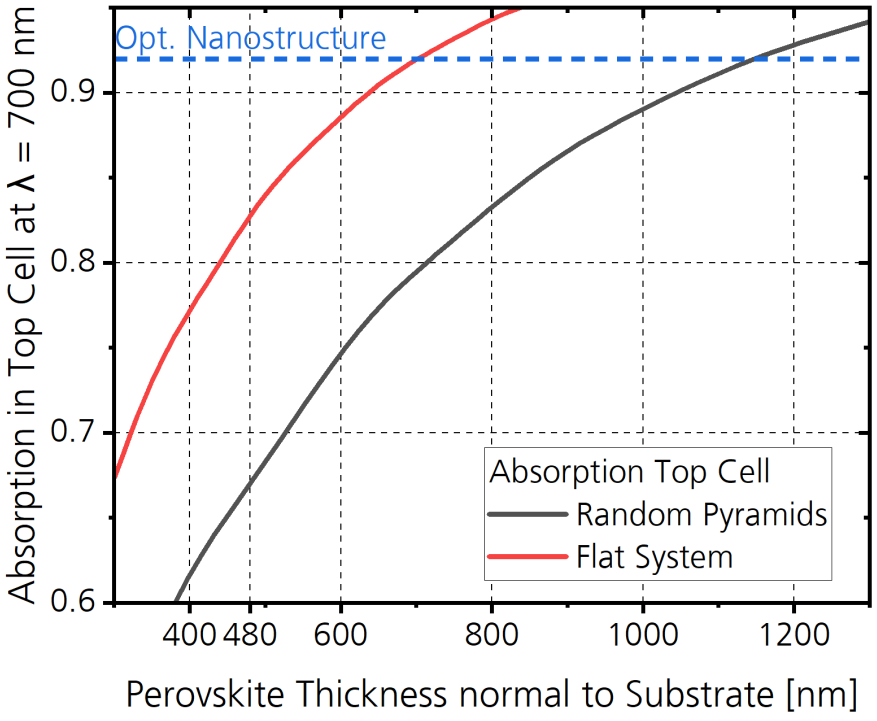

Figure S5: Absorption at 700 nm for a perovskite absorber of different thicknesses on a flat/random pyramid substrate. The thickness is measured normal to the macroscopic sample surface to provide a measure for the material volume in use.

References

1. PV Lighthouse, “Refractive index library,” https://www.pvlighthouse.com.au/refractive-index-library.
2. J. M. Siqueiros, R. Machorro, and L. E. Regalado, “Determination of the optical constants of MgF(2) and ZnS from spectrophotometric measurements and the classical oscillator method,” Applied optics 27, 2549–2553 (1988).
3. L. Krückemeier, U. Rau, M. Stolterfoht, and T. Kirchartz, “How to Report Record Open-Circuit Voltages in Lead-Halide Perovskite Solar Cells,” Advanced Energy Materials 10, 1902573 (2020).
4. J. Chantana, T. Kato, H. Sugimoto, and T. Minemoto, “Investigation of correlation between open-circuit voltage deficit and carrier recombination rates in Cu(In,Ga)(S,Se) 2 -based thin-film solar cells,” Appl Phys Lett 112, 151601 (2018).
5. S. Manzoor, J. Häusele, K. A. Bush, A. F. Palmstrom, J. Carpenter, Z. J. Yu, S. F. Bent, M. D. McGehee, and Z. C. Holman, “Optical modeling of wide-bandgap perovskite and perovskite/silicon tandem solar cells using complex refractive indices for arbitrary-bandgap perovskite absorbers,” Optics Express 26, 27441 (2018).
6. J. P. Hugonin and P. Lalanne, Reticolo software for grating analysis (Institut d'Optique, 2005).
7. T. Ameri, G. Dennler, C. Waldauf, H. Azimi, A. Seemann, K. Forberich, J. Hauch, M. Scharber, K. Hingerl, and C. J. Brabec, “Fabrication, Optical Modeling, and Color Characterization of Semitransparent Bulk-Heterojunction Organic Solar Cells in an Inverted Structure,” Advanced Functional Materials 20, 1592–1598 (2010).
8. H.-L. Chen, A. Cattoni, R. De Lépinau, A. Walker, O. Hoehn, D. Lackner, G. Siefer, N. Vandamme, J. Goyard, B. Behaghel, C. Dupuis, N. Bardou, F. Dimroth, S. Collin, H.-L. Chen, A. Cattoni, R. de Lépinau, A. W. Walker, O. Höhn, D. Lackner, G. Siefer, M. Faustini, N. Vandamme, J. Goffard, B. Behaghel, C. Dupuis, N. Bardou, F. Dimroth, and S. Collin, “A 19.9%-efficient ultrathin 205nm-thick GaAs Solar Cell with a Silver Nanostructured Back Mirror // A 19.9%-efficient ultrathin solar cell based on a 205-nm-thick GaAs absorber and a silver nanostructured back mirror,” Nat Energy 4, 761–767 (2019).
9. D. Sell, J. Yang, S. Doshay, R. Yang, and J. A. Fan, “Large-Angle, Multifunctional Metagratings Based on Freeform Multimode Geometries,” Nano letters 17, 3752–3757 (2017).
10. C. Messmer, B. S. Goraya, S. Nold, P. S. Schulze, V. Sittinger, J. Schön, J. C. Goldschmidt, M. Bivour, S. W. Glunz, and M. Hermle, “The race for the best silicon bottom cell: Efficiency and cost evaluation of perovskite–silicon tandem solar cells,” Progress in Photovoltaics: Research and Applications (2020).
11. M. A. Green, “Lambertian light trapping in textured solar cells and light-emitting diodes. analytical solutions,” Prog Photovoltaics 10, 235–241 (2002).